โครงสร้างจุลภาคสามมิติและแร่วิทยาของเนินพุโคลน บริเวณเซลทันซี รัฐแคลิฟอร์เนีย ประเทศสหรัฐอเมริกา

นางสาวบุศรินทร์ เกียรติกุลกังวาน

โครงงานนี้เป็นส่วนหนึ่งของการศึกษาตามหลักสูตรวิทยาศาสตรบัณฑิต
ภาควิชาธรณีวิทยา คณะวิทยาศาสตร์ จุฬาลงกรณ์มหาวิทยาลัย
ปีการศึกษา 2559

THREE- DIMENSIONAL MICROSTRUCTURES AND MINERALOGY OF MUD VOLCANO FROM SALTON SEA, CALIFORNIA, USA

Miss Boodsarin Keattikulkungwan

A Project Submitted in Partial Fulfillment of the Requirements
for the Degree of Bachelor of Science Program in Geology
Department of Geology, Faculty of Science, Chulalongkorn University
Academic Year 2016

Project Title	THREE- DIMENSIONAL MICROSTRUCTURES AND MINERALOGY OF MUD VOLCANO FROM SALTON SEA, CALIFORNIA, USA
By	Miss Boodsarin Keattikulkungwan
Field of Study	Geology
Project Advisor	Waruntorn Kanitpanyacharoen, Ph.D.

Submitted date.....

Approval date.....

.....

Project Advisor
(Waruntorn Kanitpanyacharoen, Ph.D.)

บุศรินทร์ เกียรติกุลกังวาน : โครงสร้างจุลภาคสามมิติและแร่วิทยาของเนินพุโคลนบริเวณเซลทันซี รัฐแคลิฟอร์เนีย ประเทศสหรัฐอเมริกา (THREE-DIMENSIONAL MICROSRUCTURES AND MINERALOGY OF MUD VOLCANO FROM SALTON SEA, CALIFORNIA, USA) อ.ที่ปรึกษาโครงงาน : อาจารย์ ดร.วรัญทร คณิตปัญญาเจริญ, 37 หน้า.

หินตะกอนที่เกิดจากการปะทุของเนินพุโคลนจะประกอบด้วยแร่ดินเป็นปริมาณมาก เนื่องจากของไหลและแก๊สที่ออกมานั้น เกิดจากชั้นหินหรือชั้นตะกอนและชั้นน้ำที่อยู่ลึกได้รับความร้อนและความดันสูง ทำให้แร่ต่างๆ แปรสภาพเป็นแร่ดินและละลายรวมกับน้ำร้อน เป็นของไหลร้อน เมื่อได้รับแรงดันเพิ่มจากกระบวนการทางธรณีสัณฐานก็จะแทรกตัวขึ้นมาตามรอยแตก หินตะกอนที่เกิดจากเนินพุโคลนมีอยู่หลายพื้นที่ทั่วโลก แต่ยังไม่ได้รับการศึกษาเป็นที่แพร่หลายโดยเฉพาะเรื่องของแร่องค์ประกอบและโครงสร้างในระดับจุลภาค เนื่องจากมีผลึกแร่ที่เล็กมากและเนื้อละเอียด ต้องใช้วิธีการศึกษาที่มีความละเอียดสูงเพื่อศึกษาข้อมูลได้อย่างแม่นยำ โครงงานนี้ได้นำตัวอย่างหิน 2 ตัวอย่างจากบริเวณเซลทัลซี รัฐแคลิฟอร์เนีย ประเทศสหรัฐอเมริกามาศึกษาแร่องค์ประกอบ ลักษณะการเรียงตัวของแร่แบบจำเพาะและโครงสามสามมิติระดับจุลภาคด้วยเทคโนโลยีขึ้นสูงของรังสีเอ็กซ์ที่ผลิตจากเครื่องเร่งอนุภาคซินโครตรอน ผลการศึกษาพบว่าแร่องค์ประกอบหลักเป็นแร่ดินประเภทแร่อิลไลต์ไมก้า, แร่สเม็กไทต์ และแร่เคโอลิไนต์ มีปริมาณแร่ดินรวมประมาณร้อยละ 69 – 75 โดยน้ำหนัก นอกจากนี้ยังพบแร่แคลไซต์และแร่โดโลไมต์ในตัวอย่างบีเท่านั้น บ่งบอกถึงความหลากหลายของแร่องค์ประกอบของของไหลร้อนที่ปะทุขึ้นมาในแต่ละช่วงเวลา จากการคำนวณการเรียงตัวแบบจำเพาะของแร่ พบว่าแร่ดินในตัวอย่างเอมีการเรียงตัวต่ำมาก ในขณะที่แร่ดินในตัวอย่างบีมีการเรียงตัวที่ดี ซึ่งสอดคล้องกับผลการวิเคราะห์โครงสร้างสามมิติระดับจุลภาค แสดงให้เห็นว่าแร่ดินในตัวอย่างบีมีการจัดเรียงตัวขนานกันในแนวระนาบได้ดีกว่าในตัวอย่างเอ โดยปัจจัยหลักที่ส่งผลกระทบต่อการจัดเรียงตัวแบบจำเพาะของแร่ดินคือ ขนาดของแร่ดินและเม็ดตะกอนทราย ตัวอย่างบีมีขนาดของแร่ดินและเม็ดตะกอนส่วนใหญ่ค่อนข้างเล็กและใกล้เคียงกันทำให้แร่ดินซึ่งมีลักษณะเป็นแผ่นเรียงตัวแบบจำเพาะได้ดีไม่ถูกกีดขวางด้วยเม็ดตะกอนขนาดใหญ่ในกระบวนการสะสมตัว และช่องว่างก็ถูกเติมเต็มด้วยเม็ดทรายหรือเม็ดแร่ขนาดเล็ก นอกจากนั้นยังพบลักษณะของรอยแตกระดับจุลภาคในทั้ง 2 ตัวอย่างซึ่งมีการวางตัวในแนวกึ่งแนวระนาบ และในตัวอย่างบีจะเห็นได้ชัดว่า รอยแตกนั้นเรียงตัวขนานไปกับการเรียงตัวแบบจำเพาะของแร่ดิน เนื่องจากรอยแตกที่เกิดขึ้นเป็นช่องว่างที่เกิดจากแร่ดินตกสะสมตัวเรียงในทิศทางเดียวกัน

ภาควิชา ธรณีวิทยา ลายมือชื่อนิสิต _____

สาขาวิชา ธรณีวิทยา ลายมือชื่อ อ.ที่ปรึกษาหลัก _____

ปีการศึกษา 2559

5632723323 : MAJOR GEOLOGY
KEYWORDS : MUD VOLCANO / CRYSTALLOGRAPHIC PREFERRED ORIENTATION / CLAY MINERALS / SALTON SEA

BOODSARIN KEATTIKULKUNGWAN : THREE- DIMENSIONAL MICROSTRUCTURES AND MINERALOGY OF MUD VOLCANO FROM SALTON SEA, CALIFORNIA, USA, ADVISOR : WARUNTORN KANITPANYACHAROEN, Ph.D., 37 pp.

Mud volcano is a unique geological formation that constantly ejects clay-rich fluids and gases to the surface. These fluids is generally formed due to the mixing and heating process between rock or sediment layers and subsurface water. Over time clay-rich fluids can become overpressured and be forced upward through fractures in the overlying rocks when experience extremely high pressure from tectonic activities in the area. Despite the abundance of sedimentary rocks formed by mud volcano activities worldwide, their physical and chemical properties are still poorly understood. This is mainly due to the extremely fine grain size of clay minerals, which cannot be effectively characterized by classical methods. This study thus aims to determine mineral compositions, crystallographic preferred orientation (CPO), and microstructures of 2 sedimentary samples obtained from mud volcano near the Salton Sea in California, USA by using synchrotron X-ray techniques. Results from synchrotron X-ray diffraction show that both samples have high clay content approximately 69 – 75wt.%, including illite-mica, smectite, and kaolinite as major phases. A small amount of calcite and dolomite are only observed in Sample B, indicating a compositional variation of fluids ejected from different periods of the same mud volcano. Despite a slight compositional difference, these samples have a noticeable variation of microstructures. Sample A has very weak degrees of clay preferred orientation (1-2 m.r.d.) while Sample B has moderate degrees of preferred orientation (~3 m.r.d.). These results are consistent with three-dimensional morphology and distribution of clay minerals obtained from synchrotron x-ray microtomography measurement as most of clay particles in sample B are very fine and preferentially align parallel to sub-parallel to the horizontal direction. On the contrary, clay particles in sample A are mostly randomly orientated. Due to the grain size effect. Sand- or silt-size particles in the matrix play a major role in controlling the preferred orientation of sheet-like clay particles during sedimentation.

Department : Geology Student's Signature
Field of Study : Geology Advisor's Signature
Academic Year : 2016

Acknowledgments

This senior project could not be successfully completed without the helping and support from everyone. First and foremost, I would like to express my gratitude to my senior project advisor, Dr.Waruntorn Kanitpanyacharoen, who gave all helpful helping and excellent advice since the project started until successfully completed for almost one year.

I would like to express my deeply thanks to the Advance Protron Source, Argonne National Laborytory for laboratory analyzing.

The special thanks to Mr. Jiraphat Charoensawan who taught me to use MAUD software and good suggestion as well.

Finally, my achievement would not be completed without Department of Geology, Chulalongkorn University, and also taken care from all of professors.

Contents

List of tables

List of figures

Chapter 1
Introduction

1.1 Background

Mud volcano refers to a geological formation created by an expulsion of hot and highly-pressured fluids and gases. The expulsion occurs when subsurface clay-rich sediments or rocks experience high temperature and pressure. These materials are then partially melted and mixed into clay-rich fluids. Hot fluids and gases can be forced upward due to many tectonic processes such as overpressure, fault movement, and plate subduction. The fluids slowly cools down on the surface (Figure 1.1) while releases a significant amount of volatiles and gases such as methane and carbon dioxide after the expulsion. Minerals, sediments, and particles also are settled out from the fluids, starting the sedimentation process. The formation process of sedimentary rocks from mud volcano is quite different from those of other clay-rich rocks such as shale and mudstone, which are normally deposited in the subsurface. There are many mud volcano around the world including USA, Indonesia, Burma, Iran, Spain, and Columbia just a few names of the countries. Most appear in Eastern Azerbaijan and some are related structural trap for petroleum. Fowler et al. (2000) studied about mud volcano and structural development on Shan Deniz where the largest natural gas in Azerbaijan. Also, studied about fluid evolution and authigenic mineral paragenesis related salt diapirism by Haffer et al. (2013). Because mud volcano is linked to fluids in deep subsurface. Despite the abundance of mud volcano worldwide and their association with geothermally-active areas, their physical and chemical characteristics are poorly understood. This study thus aims to investigate mineral composition, crystallographic preferred orientation (CPO), and three-dimensional microstructures of mud volcano and to establish a better understanding of their sedimentation process.

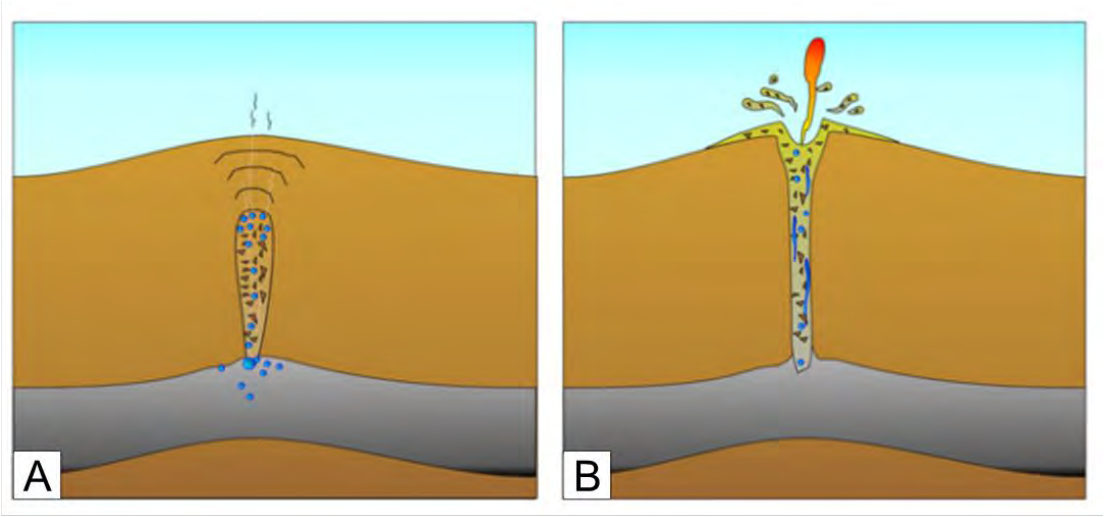

Figure 1.1: A sketching growth model of mud volcano, (A) clay-rich fluids can become overpressured and be forced upward through fractures in the overlying rocks and then (B) the fluids slowly cools down on the surface. (Modified from Mazzini, 2009).

Preferred orientation refers to minerals align parallel to each other in the same direction for example in metamorphic rocks. During metamorphism process, stress can flatten grains in the rocks to sheet-like grains then it preferentially oriented perpendicular to the direction of maxima compression. The results of orientation in metamorphic rock are shown as foliation. But some minerals such as clay minerals which are sheet-like shape, can align during sedimentation, compaction, and deformation. Both bedding plane and cleavage are dominant with c-axis (001) (Kanitpanyacharoen et al., 2012).

Clay minerals are common hydrothermal alteration minerals or weathering products from feldspars. Clay's size are usually less than 2 micrometers, it is difficult to determine their crystallographic preferred orientation with classical method. So it may need special analytical techniques to study, such as scanning electron microscopy (SEM), transmission electron microscope (TEM).

As previous study of crystallographic preferred orientation of clay minerals in shale and other clay-rich rocks used new methods with synchrotron X-ray Diffraction (Syn-XRD) to characterize composition as well as textures. With high energy source of Synchrotron X-rays, can quantify degree of crystallographic preferred orientation (CPO) shows as pole figure which analyzed by Rietveld analysis (Rietveld, 1969) in the software MUAD (Lutterottiet et al., 1997). Wenk et al. (2009) compared preferred orientation of phyllosilicates in fault gouge, shale, and schist with Synchrotron X-ray techniques. Clay fabrics in fault gouge are weak, those in shale are moderate

(Figure 1.2), and strongest in schist. Additionally, Janssen et al. (2012) about fault gouge from San Andreas Fault Observation Depth (SAFOD) samples mainly contain quartz and clay minerals with very weak degrees of preferred orientation of clay minerals. The results are measured by using Syn-XRD method.

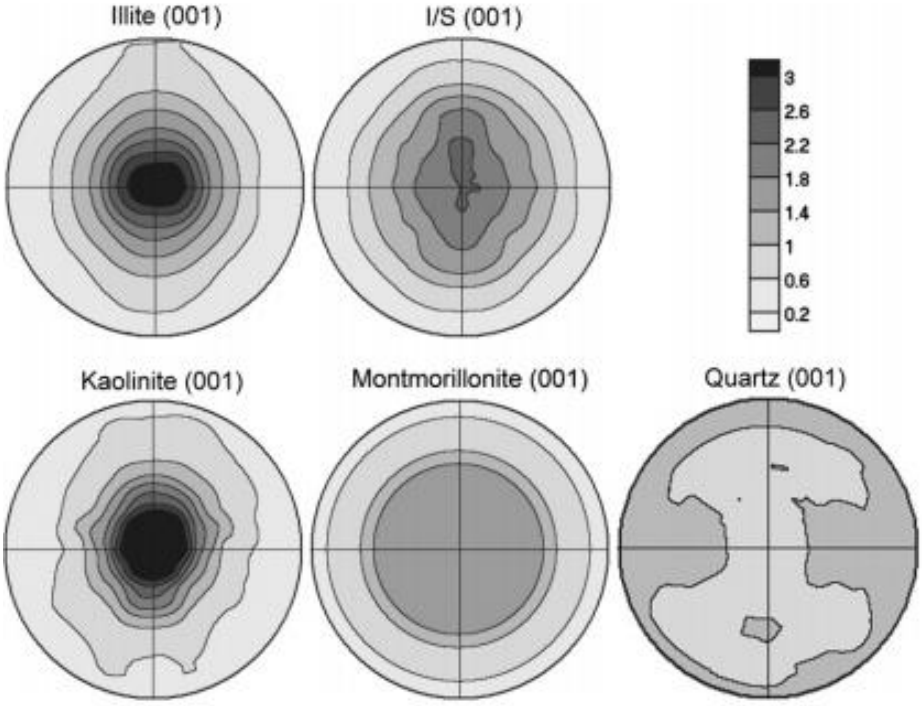

Figure 1.2: A pole figure of shale, showing orientation of illite, illit-smectite, kaolinite, montmorillonite, and quartz. Projection perpendicular to bedding plane.

For three-dimensional of microstructures at micro scale were investigated by using synchrotron X-ray tomography (Syn-XTM) and generated model by using segmentation program. Gilani et al. (2014) used Syn-XTM to analyze and investigate 3D structure of wood and the distribution of fungi (Figure 1.3). Not only analyze wood but also the rocks. Worked by Kanitpanyacharoen et al. (2012) using Syn-XRD and SYN-XTM to compare preferred orientation of minerals and microstructures in shale with different thermal maturity. The results show that clays have high degrees of preferred orientation while calcite, dolomite, and pyrite have a weak. Also, Syn-XTM show about 3D microstructures distribution for example pore, kerogen, clay minerals (Figure 1.4).

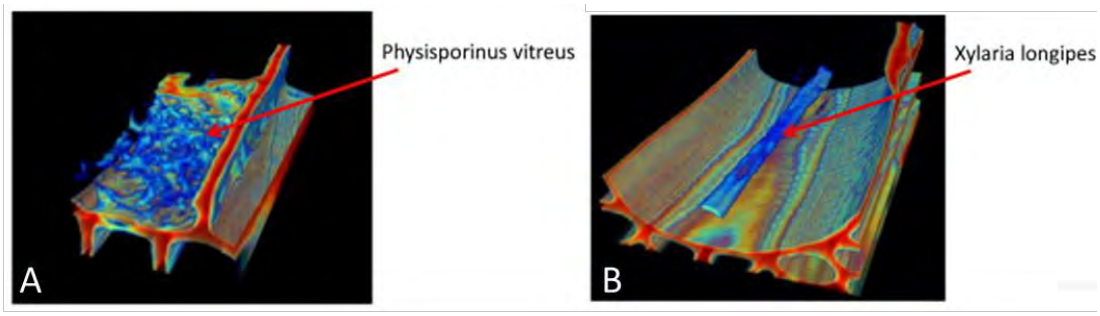

Figure 1.3: A 3D rendering of (A) the network of *Physisporinus Vitreus* (88x60x150 μm^3) and (B) single hypha of *Xylaria longipes* (100x70x150 μm^3) (Gilani et al., 2014)

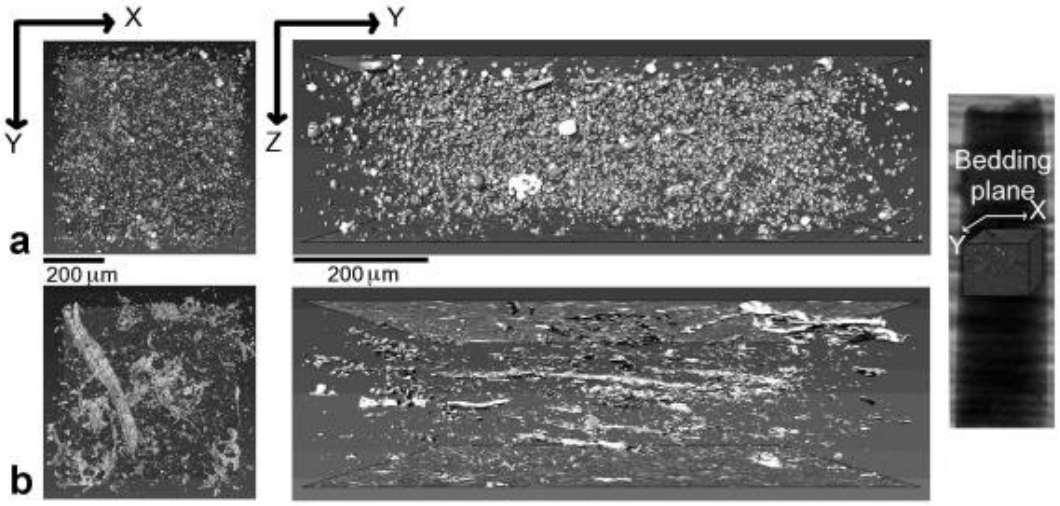

Figure 1.4: A 3D microtomography images show the distribution of (a) pyrite and (b) micropores, fractures, and kerogen. (Kanitpanyacharoen et al., 2012)

This study will use these 2 methods to determine mineral composition as well as preferred orientation of minerals. In addition, analyze three-dimensional of microstructures distribution.

1.2 Objectives

The goals of this study are to identify the mineral compositions and mineral preferred orientation of sedimentary rocks obtained from mud volcano and to investigate three-dimensional microstructures for establishing a better understanding of their sedimentation process.

Chapter 2

Study area

2.1 Geological setting

Salton Sea is pull-apart basin in southern California (Figure 2.1) which formed by oblique extension across strike-slip fault systems (Brothers D. N. et al., 2009). The two dominant faults are San Andreas Fault (SAF) and Imperial Fault (IF). Salton Sea started to extend ~0.5 million years ago (Brothers D. N. et al., 2009). Earlier, blocks between San Andreas Fault (SAF) and San Jacinto Fault (SJF) are rotated by dextral shear (Figure 2.3a). At present, model of pull-apart basin is shown in Figure 2.3b and this area is high subsidence, high thermal anomaly with a heat flow up to 600 mWm^{-2} (e.g., Helgeson,1968; Robinson et al., 1976; Lachenbruch et al., 1985; Williams,1997) and the quaternary volcanic intrusions (Figure 2.4). The intrusions significant focused and diffused CO_2 degassing (Kerrick et al., 1995). The sediments deposits in Salton Sea are lacustrine interbedded with fluvial deposits within a 6000 m thickness which sediments are transported by Colorado river (Waters 1981). Sediments deposited during the late Holocene in lake are shown in Cahuilla Formation (CFm) (Figure 2.4) (Brothers D. N. et al., 2009). The sedimentary packages in this formation record shoreline fluctuation for at least 12 transgression-regression cycles (Brothers D. N., et al., 2009). The Pleistocene Brawley Formation underlay the CFm (Figure 2.4) which is Colorado river deltaic sediments (Brothers D. N. et al., 2009). These sediments are placed on top of evaporite deposits. Believe that CO_2 come from the deep subsurface where it is the product of metamorphic decarbonation reaction at temperature at least 125°C (Muffler and White, 1969). The water in Salton Sea is high salinity due to the deep hydrothermal fluids dissolved the evaporites by high-temperature interaction between fluids and rocks (Helgeson, 1968). Mud volcano area in Salton Sea is located in southern part (yellow pin at Figure 2.1). This area called Salton Sea Geothermal System (SSGS). The surface expressions of the Salton Sea Geothermal System are appeared to be the mud volcano. Not only mud volcano, but also seeps are located along the edge of the Salton Sea.

Figure 2.1: A map of Salton Sea, which is located directly on the San Andreas Fault. Yellow pin indicates mud volcano area.

Figure 2.2: A field of mud volcano at the Salton Sea location. (image source: https://www.tripadvisor.com/LocationPhotoDirectLink-g32784-d5533663-i127574636-Salton_Sea_Mud_Volcanoes-Niland_California.html)

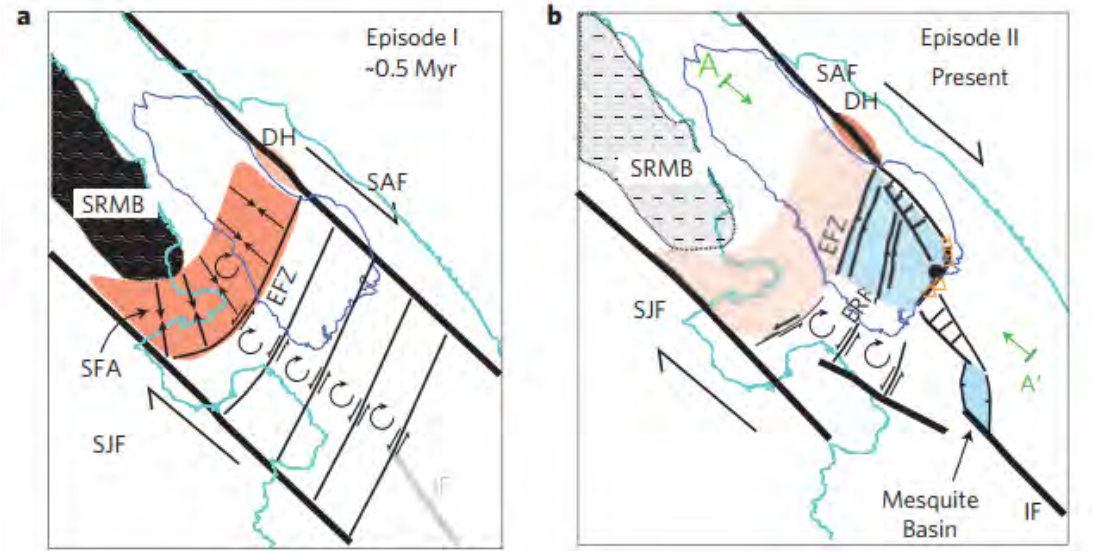

Figure 2.3: A models for the tectonic evolution of the Salton Sea. Abbreviations: SRMB, Santa Rosa mountain block; SJF, San Jacinto fault; EFZ, Extra fault zone; ERF, Elmore Ranch fault; BSZ, Brawley seismic zone; SAF, San Andreas fault; SHF, Superstition Hills fault; SMF, Superstition Mountain fault; IF, Imperial fault; DH, Durmid Hill; SFA, San Felipe anticline; MB, Mesquite basin (a) The block between SAF and SJF are rotated by dextral shear. (b) Present model of pull-apart basin. (Brothers D. N. et al., 2009).

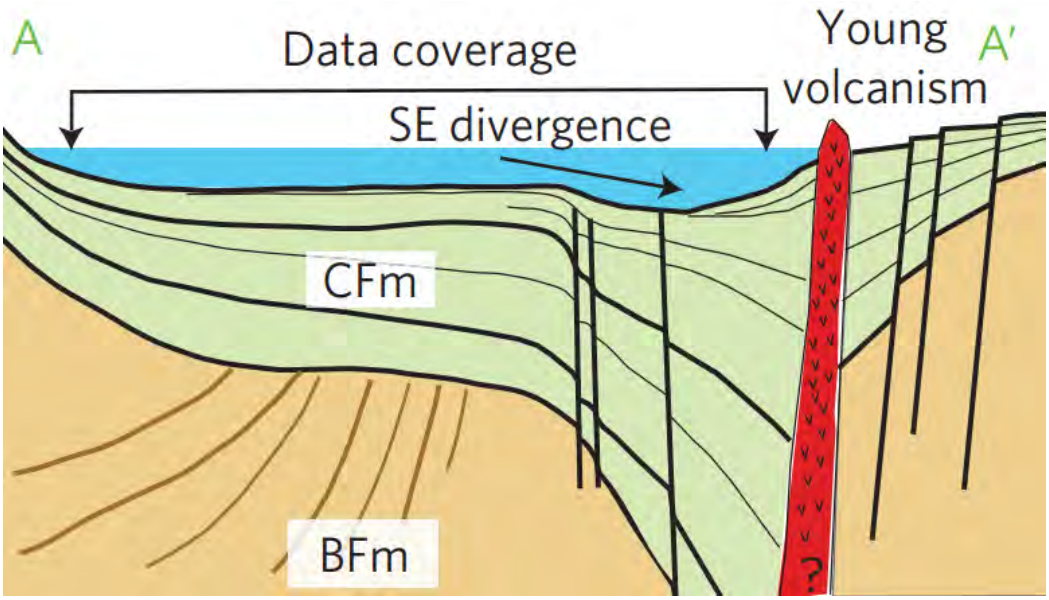

Figure 2.4: A cross-section (from Figure 2.2b) of Salton Sea by seismic interpretation, CFm refers to Cahuilla Formation which is sediments deposit during Holocene and BFm means to Brawley Formation which is Pleistocene rocks (Brothers D. N. et al., 2009)

From study about the San Andreas Fault system by Irwin 1990 show that due to the Pacific plate oblique subducted beneath the North American plate in late Eocene, the San Andreas Fault was born in between plate boundary. Before then, Farallon plate which is another oceanic plate was subducted beneath the North American plate (Irwin 1990). The two plates were sliding past each other in early Miocene age, instead of colliding, so a transform fault was occurred in this boundary called a strike slip fault (Figure 2.5) (Irwin 1990).

Measurements of rocks offset is approximately 214 kilometers across both sides of the fault and total displacement along the fault is at least 563 kilometers since it formed (Irwin 1990). The length of San Andreas Fault is about 1,287 kilometers, stretching from the Mendocino coast south to the San Bernardino Mountains and the Salton Sea. It was divided into northern and southern segments, separated from central because of a continuous creeping (Irwin 1990).

The San Andreas Fault was generated lots of earthquakes in California. So, the scientists drilled into Earth's crust to study about fault depth, rocks and their behavior to predict the earthquake.

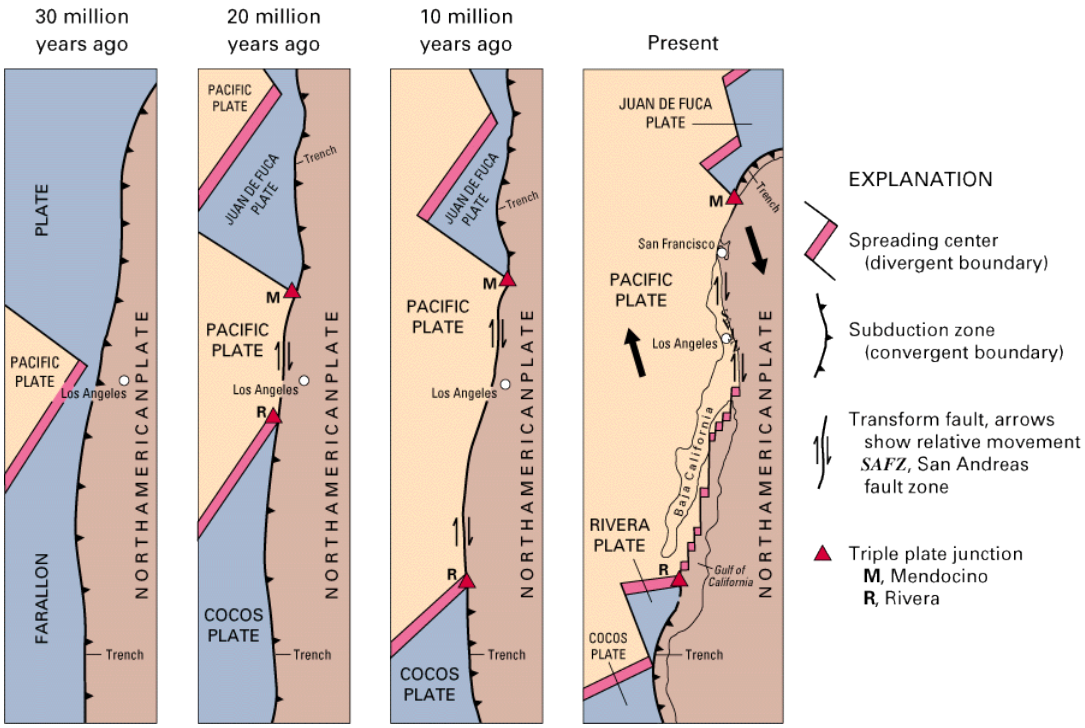

Figure 2.5: A schematic evolution of San Andreas Fault in California, USA (image source: http://pubs.usgs.gov/gip/dynamic/tectonic.html)

Chapter 3

Methodology

The 2 samples were collected from mud volcano area in Salton Sea, California, USA. We aim to study about mineralogy and microstructures. To determine mineral composition and crystallographic orientation of minerals using high-energy Synchrotron X-rays. Diffraction data were further analyzed by MAUD program. Microstructures were analyzed by using Synchrotron X-ray Microtomography.

3.1 Synchrotron X-ray Diffraction

Firstly, to identify mineral compositions and determine lattice preferred orientation of minerals, we used hard synchrotron X-ray diffraction from BESSRC 11-ID-C beamline of the Advance Proton Source (APS) at Argonne National Laboratory.

Syn-XRD relies on Bragg's law.

$$2dsin\theta = n\lambda$$

Where d is d-spacing, θ is scattering angle, n is positive integer and λ is wavelength of X-ray beam. Due to each mineral has different d-spacing (d) so we identify mineral composition by using their d-spacing.

Because of non-destructive Syn-XRD experiments, we can determine lattice preferred orientation of minerals as well. Two samples were cut into cylinder of 1.5 X 1.5 millimeters in size. Then the samples were set onto a rotatable plate aligned perpendicular to the X-ray beam. A wavelength of monochromatic Synchrotron X-ray beam is 0.107980 °A. X-ray were transmitted from samples to Mar345 detector which positioned 2 meters away from samples. Diffraction images were recorded for 60 seconds as a 2θ angle range from 0-4.6° called Debye ring (Figure 4). The variation of intensity along some Debye ring can represent the preferred orientation, higher intensity along diffraction rings refer to more lattice plans aligned in that direction (Figure 3.2). Each sample was recorded 7 images in a different angle from -45° - 45° with 15° increment (-45°, -30°, -15°, 0°, 15°, 30°, 45°) to create pole figure reconstruction.

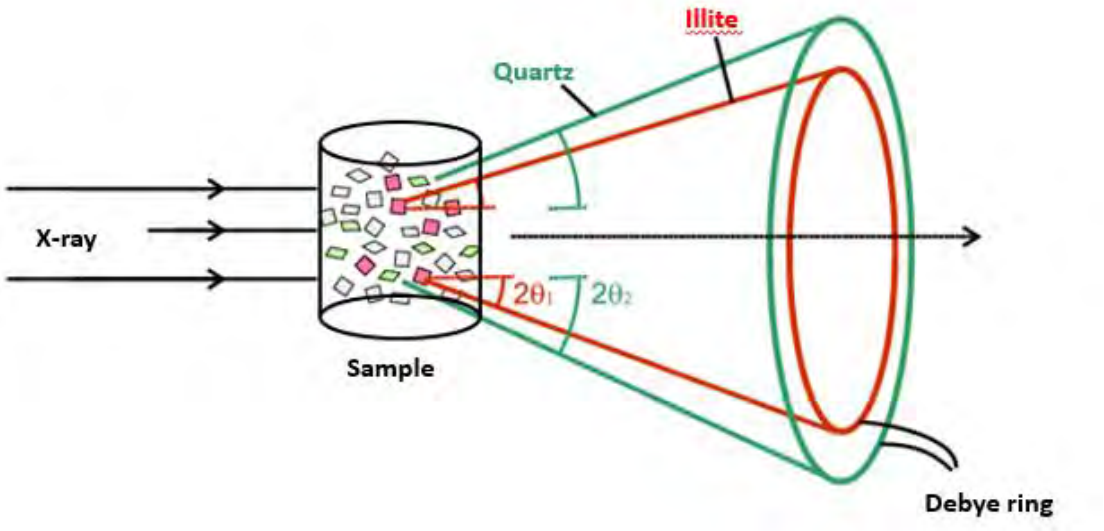

Figure 3.1: A schematic detail of Synchrotron X-ray Diffraction method. (image source: http://pd.chem.ucl.ac.uk)

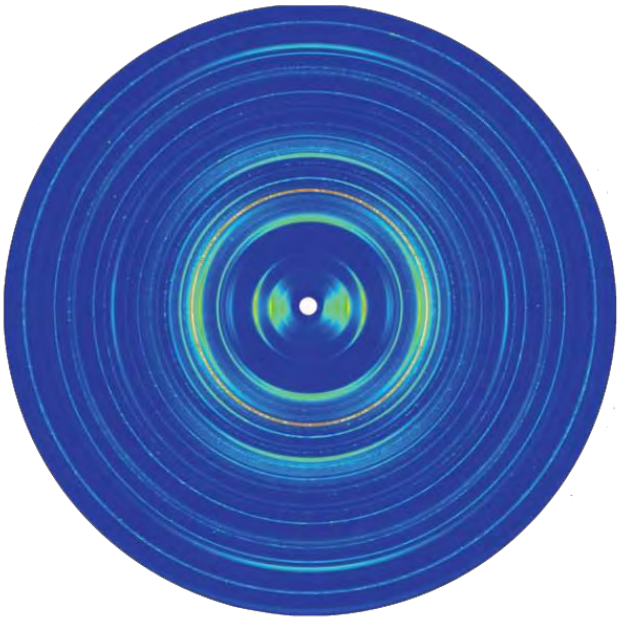

Figure 3.2: An example of diffraction image data which show the variation of intensity along each circle, higher intensity along diffraction rings refer preferred orientation of minerals (Wenk et al., 2008).

After collected diffraction image from Syn-XRD experiment then processed the data with Material Analysis Using Diffraction (MAUD) software. This software relies on Rietveld code, uses a least-square method to minimize the difference diffraction between experimental data and calculated model. So we used MAUD for quantitative data analysis by these steps.

1. Calibrate instrumental data (sample-detector distance, wavelength, beam center and image plate tilt) with CeO_2 powder standard.
2. Import one of seven diffraction image data and edit omega angle accordingly to the angle of the data.
3. Import crystallographic structures of mineral compositions which depend on peak of position. Spectrum data are displays as Q-spacing ($Q = 2\pi/d$) in order to clearly distinguish peak position.
4. Generate background binomial peak.
5. Free background and parameters and then refine background and all parameters.
6. Edit microstructure for clay mineral phase. Change c-axis instead of b-axis.
7. Refine microstrain and isotropic crystallite for clay mineral phase for the peak shapes and widths.
8. Refine bound B-factor parameters.
9. Repeat step 2-8 on the other data.
10. Combine seven diffraction image with all parameters into one.
11. Refine texture phase by using E-WIMV with angular resolution 15° of orientation distribution function (ODF).
12. Refine until calculation data are closely similar to experimental data.
13. Plot texture as pole figure reconstruction and export data.

3.2 Synchrotron X-ray microtomography

Secondly, to investigate 3D of microstructures, we used synchrotron X-ray microtomography method. This method is a non-destructive and high resolution which relies on Beer-Lambert law relates the attenuation of light to properties of material.

First step, several dark field images were collected without X-ray and bright filed images were collected with X-ray but no sample. Both images were used for correction. The sample were cut into cylinder 1 x 5 millimeters in size. Then, set the vertical axis on a rotatable plate and middle of the field of view. Samples were recorded every 0.120° until 180°. The transmitted X-ray was converted to visible light by scintillator (Figure 3.3).

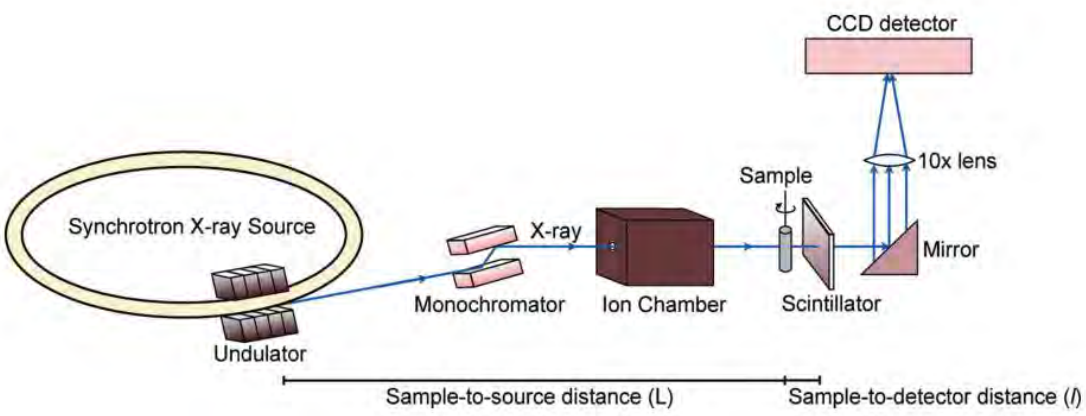

Figure 3.3: A Schematic diagram of the Synchrotron X-ray Microtomography experiment (Kanitpanyacharoen et al., 2012).

The raw projection images were reconstructed by several steps. First, removed noises which effected X-ray fluctuation by this equation.

$$Ic = (Is - Id)/(Ib - Id)$$

where I_c is the corrected image, I_b is the bright-field image, I_d is the dark-field image and I_s is the raw projection of sample (Wang *et al*., 2001) Next, Normalized the corrected images by choosing area without sample in the images and rearranged into a sinogram which contains all horizontal information of projection. Finally, reconstructed the data by using the filter black-projection into cross section image with 2048 x 2048 in pixels size for future processing.

In this study, 3D tomographic segmentation data were processed by segmentation program by these following steps.

1. Import raw images into program by setting voxel size as 0.69 micrometers and grey scale 8-bit.
2. Choose the interest area.
3. Apply 3D median filter to avoid unnecessary blurring.
4. Classify materials based on grey scale value (Table 3.1), shape, and size. Microfractures in sample are low X-ray absorption area which displayed as black. Intermediate grey shade approximately 90 vol.% represent quartz, calcite, dolomite and clay minerals. With the limit of resolution, it's hard to separate each mineral then use the value which most suitable in each sample. The high-absorbing materials are mainly pyrite according to Iron mineral compound.
5. Investigate 3D volume rendering of segmented components.

Table 3.1: A Grey scale value which used to classify materials.

Materials	Sample A	Sample B
Fracture	0-40	0-40
Clay minerals	85-110	115-130
Pyrite	190-255	190-255

Chapter 4

Results

4.1 Synchrotron X-ray Diffraction

The main objective of Syn-XRD method is to determine mineral compositions as well as preferred orientation of clay minerals. Diffraction data have been analyzed in MAUD program. The diffraction spectra (Figure 4.2-4.3) which calculated data (upper) excellently fits with experimental data (lower) in terms of intensity and peak position. The variation of intensity along the azimuth in figure 4.2-4.3 indicated the preferred orientation of some minerals e.g. smectite, illite-mica, and kaolinite. Phase of minerals composition are shown as figure 4.1. Supporting accuracy with R% values, 9% and 12% in sample A and B, respectively. The components are summarized in Table 4.1. A large proportion components in both samples is clay minerals, approximately 69 – 75 wt.% with major phases as illite-mica, smectite, and kaolinite. The amounts of other phases such as quartz and plagioclase are quite similar. In addition, calcite and dolomite are only observed in sample A with 8.12 wt.% and 1.62 wt.%, respectively.

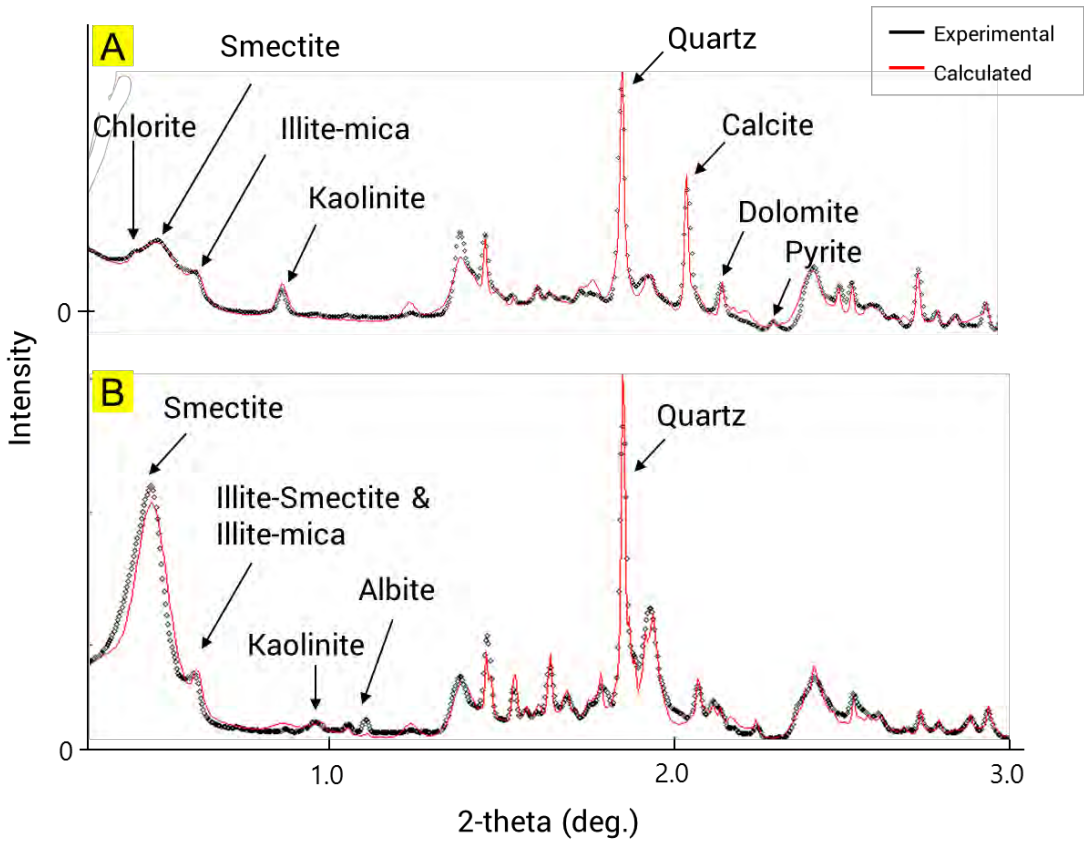

Figure 4.1: A diffraction patterns of (A) sample A and (B) sample B. Red line is calculated data, black line is experimental data both are excellent similarity.

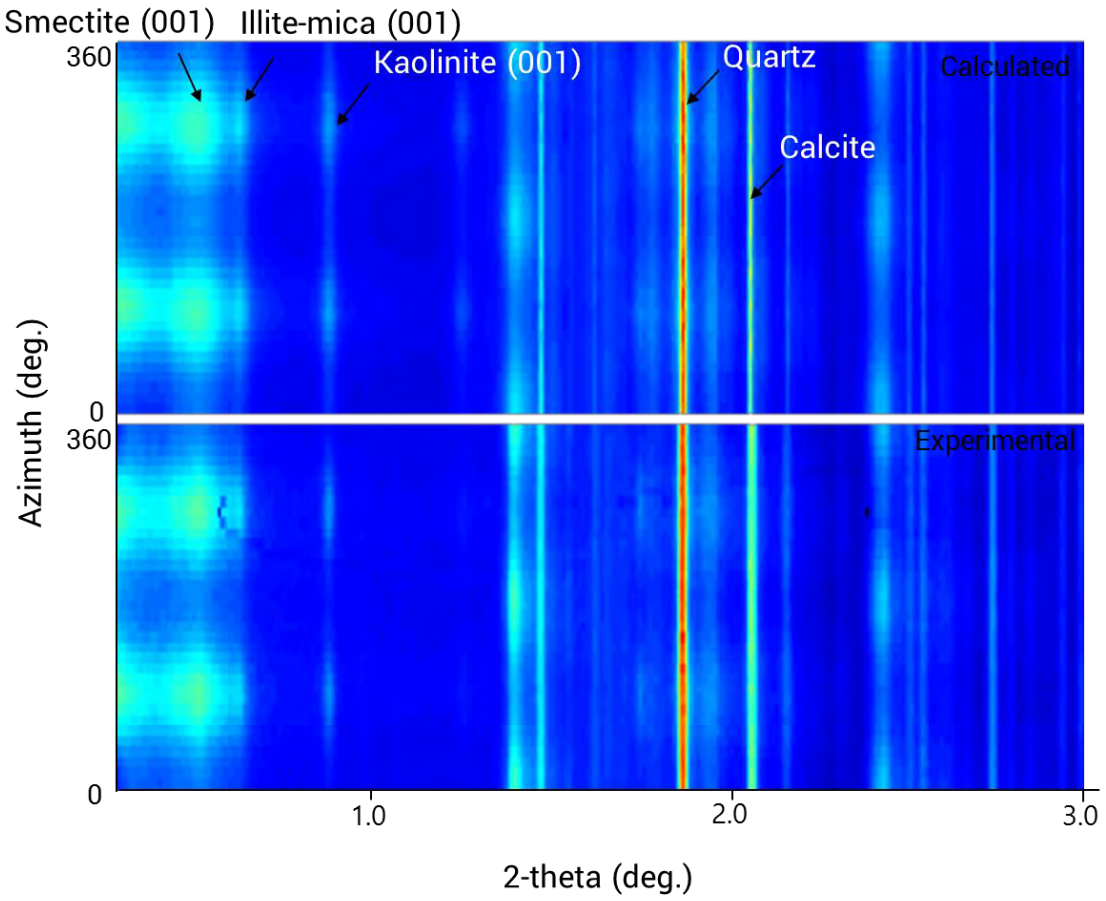

Figure 4.2: A plot 2D map of sample A which compares diffraction spectra, experimental data (above) and calculated data (below). The variation of intensity along the azimuth indicated the preferred orientation for some minerals (e.g. smectite illite-mica, kaolinite).

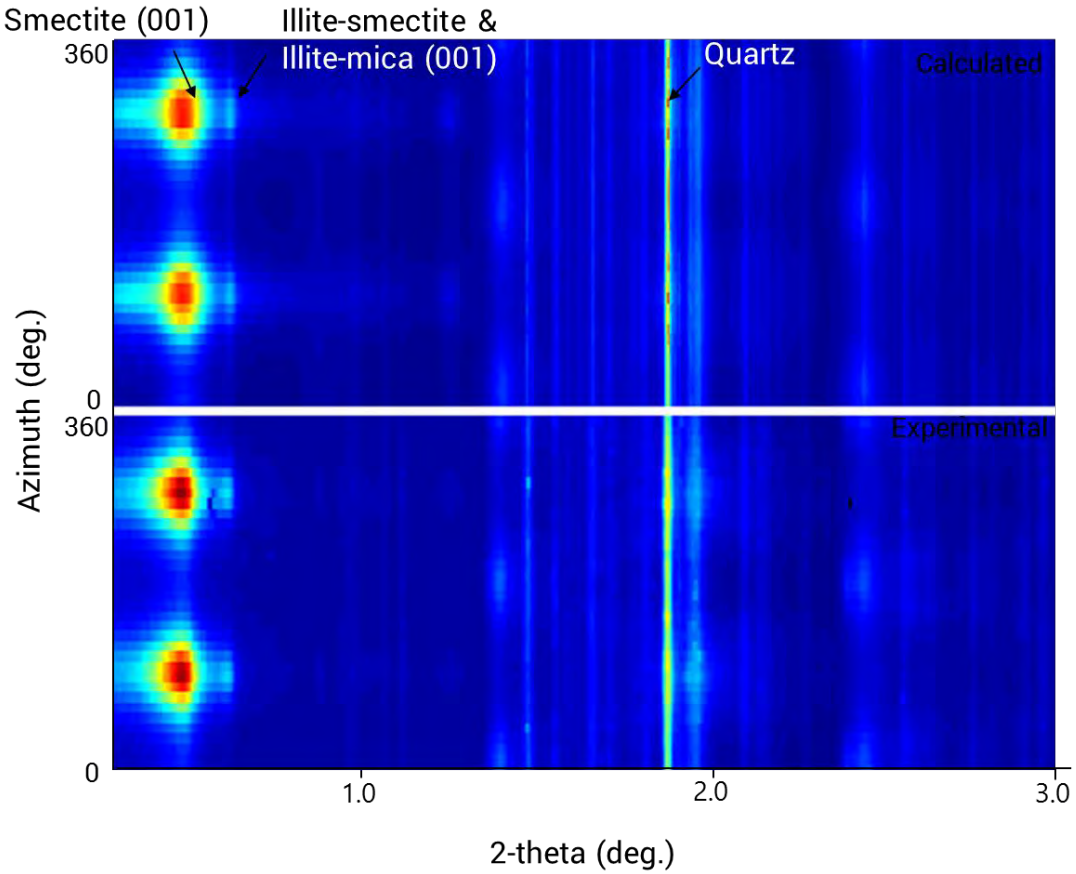

Figure 4.3: A plot 2D map of Sample B which compares diffraction spectra, experimental data (above) and calculated data (below). The variation of intensity along the azimuth indicated the preferred orientation for some minerals (e.g. smectite illite-mica, illite-smectite).

Table 4.1: A mineral compositions in weight% fraction.

Mineral compositions (wt.%)	Sample A	Sample B
Illite-mica	56.06	34.87
Illite-smectite	-	10.93
Smectite	6.31	12.46
Kaolinite	9.86	10.74
Chlorite	2.4	-
Quartz	12.82	8.96
Plagioclase	2.49	12.19
K-feldspar	-	9.82
Calcite	8.17	-
Dolomite	1.62	-
Pyrite	0.27	-

For preferred orientation of clay minerals, are shown as pole figure coverage which generates by plot c-axis (001) perpendicular to lattice plane (Figure 4.4) of different angle diffraction data from -45° - 45°. The Pole densities are shown as multiples of a random distribution (m.r.d.) which 1 m.r.d. refer to minerals are random orientation.

The pole figures of preferred orientation analysis are presented by illite-mica, illite-smectite, smectite, kaolinite, and chlorite (Table 4.2-4.3). Sample A has very weal degrees of clay preferred orientation with maximum around 1.6 m.r.d. and minimum around 0.7 m.r.d., show that most of clay minerals are close to random. On the contrary, sample B has a moderate degrees of clay preferred orientation with average about 3.2 – 3.6 m.r.d.

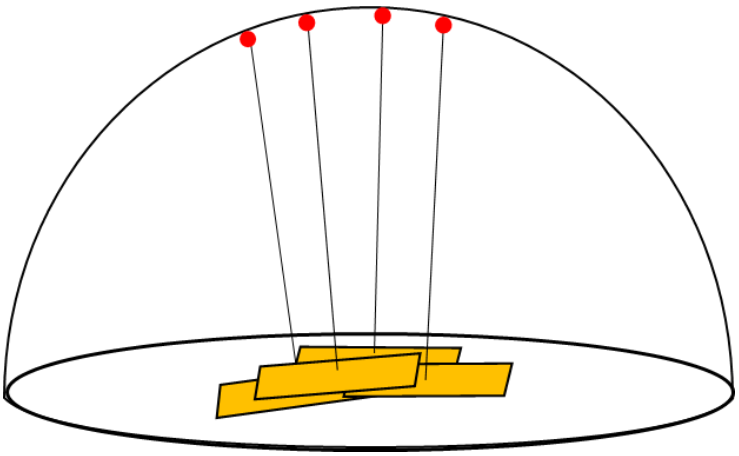

Figure 4.4: A sketching model of pole figures which projected on the lattice plane perpendicular to the center of the pole figures.

Table 4.2: A pole figure of clay minerals in sample A

Minerals	(100)	(001)
Illite-mica	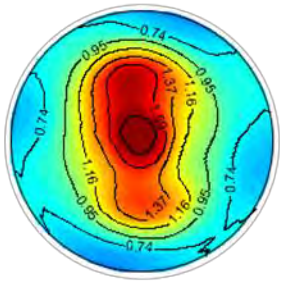	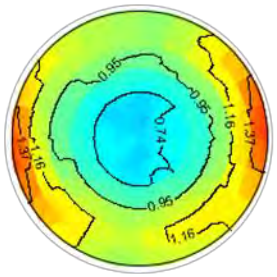
Smectite	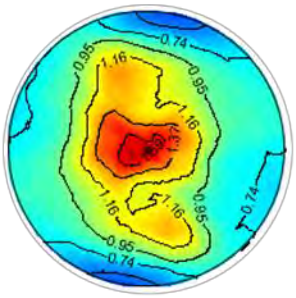	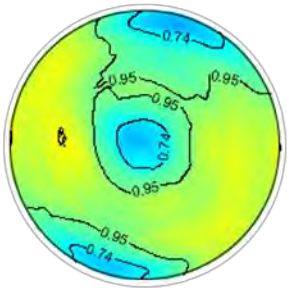
Kaolinite	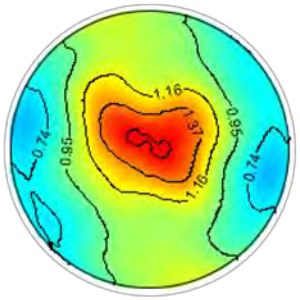	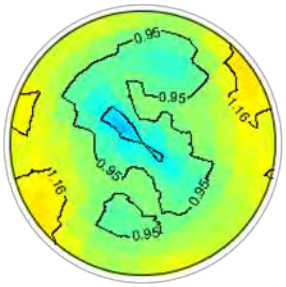
Chlorite	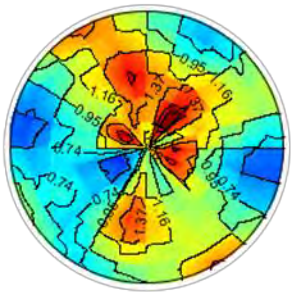	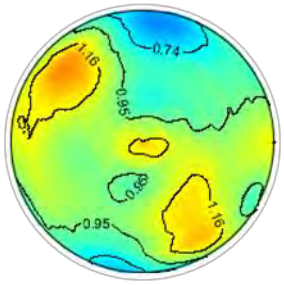

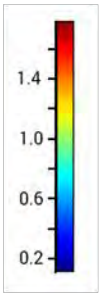

Table 4.3: A pole figure of clay minerals in sample B

Minerals	(100)	(001)
Illite-mica	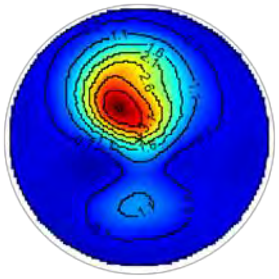	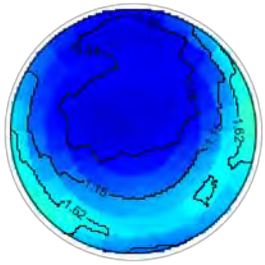
Smectite	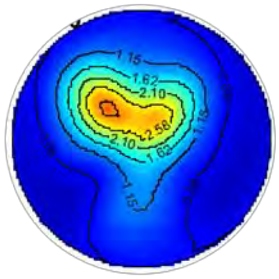	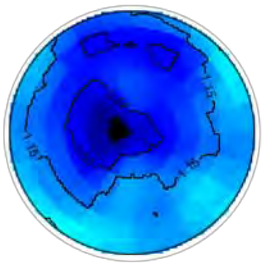
Kaolinite	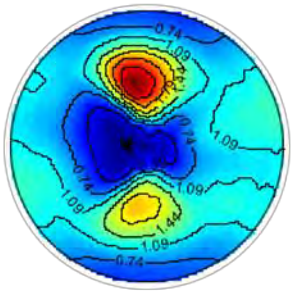	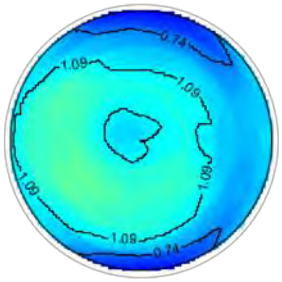
Illite-smectite	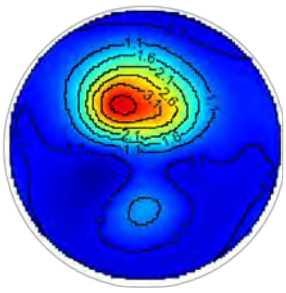	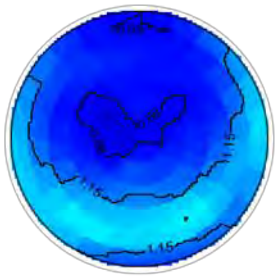

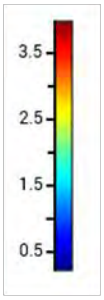

4.2 Synchrotron X-ray Microtomography

Selected area with volume of 900 x 900 x 300 voxels inside the cylinder was analyzed by segmentation program (Figure 4.5A). Materials in sample (Figure 4.5B) are classified by grey scale values due to differences of X-ray intensity absorption. Because of area without sample, microfractures are low intensity of X-ray absorption then they are very low of grey scale values (0 - 40). While pyrites which are iron mineral compound, show as very bright area because high values of grey scale. For clay minerals are hardly to classify by only grey scale values according to their chemical compositions are very similar, so we need to identify by shape of grains as well. The total volume of each materials is summarized in table 4.4. The results show that the high absorption materials in both samples are pyrite and the distribution of these minerals dose not relate with bedding plane (Figure 4.8). For intermediate shade of grey scale represented quartz, clay minerals, calcite, and dolomite, are about 90 vol.% but with limit of the resolution clay minerals are classified as 0.34vol.% and 1.44vol.% in sample A and B, respectively. Clay particles in sample A are distributed around the sample (Figure 4.6A) while aligned in the same direction in sample B (Figure 4.6B). Moreover, the 3D results also show about the sheet-like clay particles as well (Figure 4.6B). A subhorizontal microfractures are observed in both samples (Figure 4.7), which are probably results of spaces between sheet-like clay particles during sedimentation process. Supporting with results from sample B clearly show that sheet-like clay particles and microfractures are aligned parallel to each other (Figure 4.9). According to the limitation of resolution in this method, only volume percentage of microfractures with larger than micron-scale are acceptable. For clay minerals does not represent the total content.

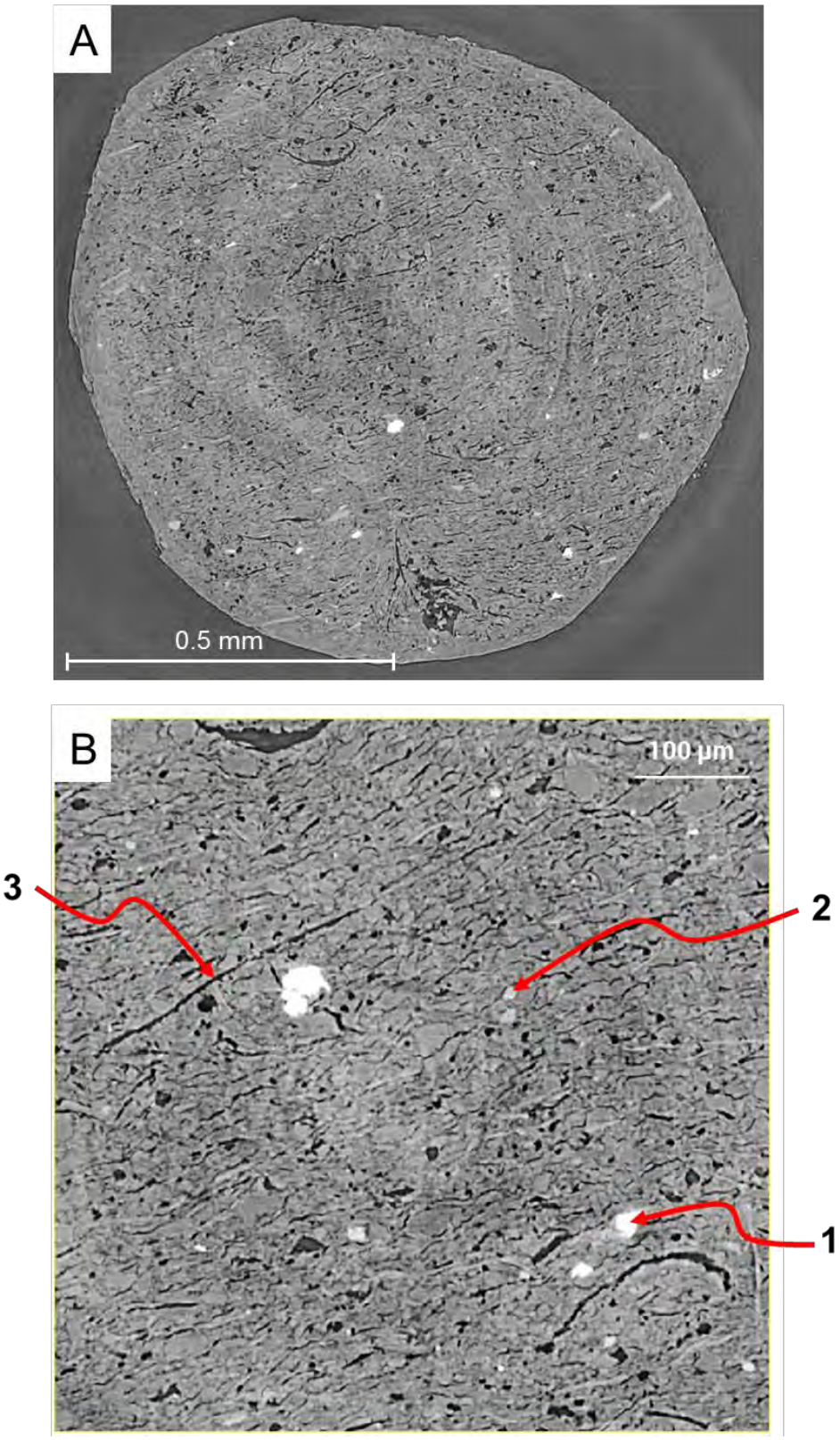

Figure 4.5: An example of microtomographic data,(A) shows the cylinder data with the area of interested inside the rectangle. (B) show area of interested with (1) pyrite, (2) clay minerals, (3) microfractures.

Table 4.4: A total volume of each materials in both sample.

Materials (Vol.%)	Sample A	Sample B
Clay minerals	0.34	1.44
Microfractures	0.12	1.72
Pyrite	0.02	0.11

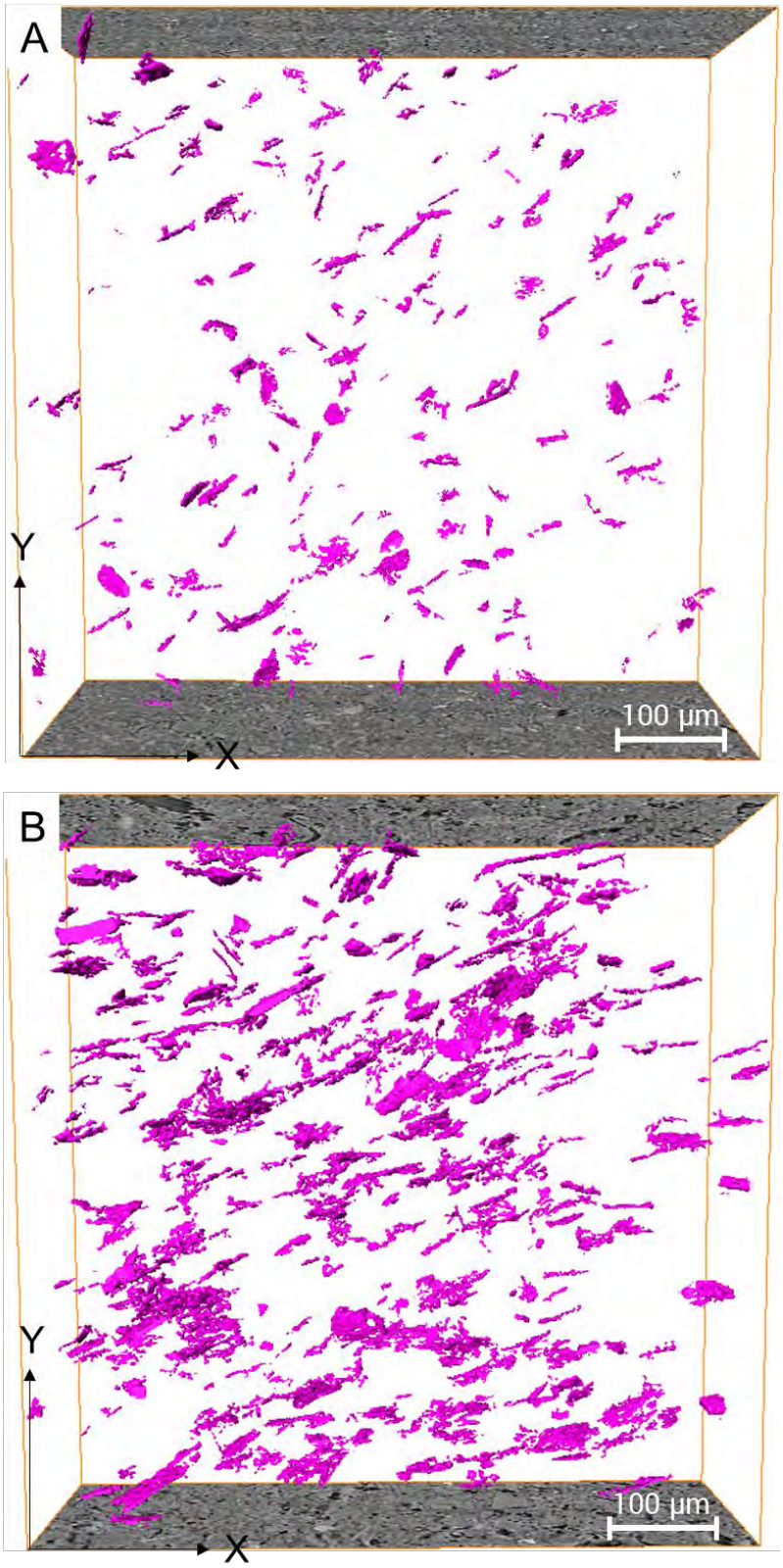

Figure 4.6: 3D distribution of clay minerals in YX section, (A) clay particles in sample A are distributed around the sample while (B) are aligned in the same direction.

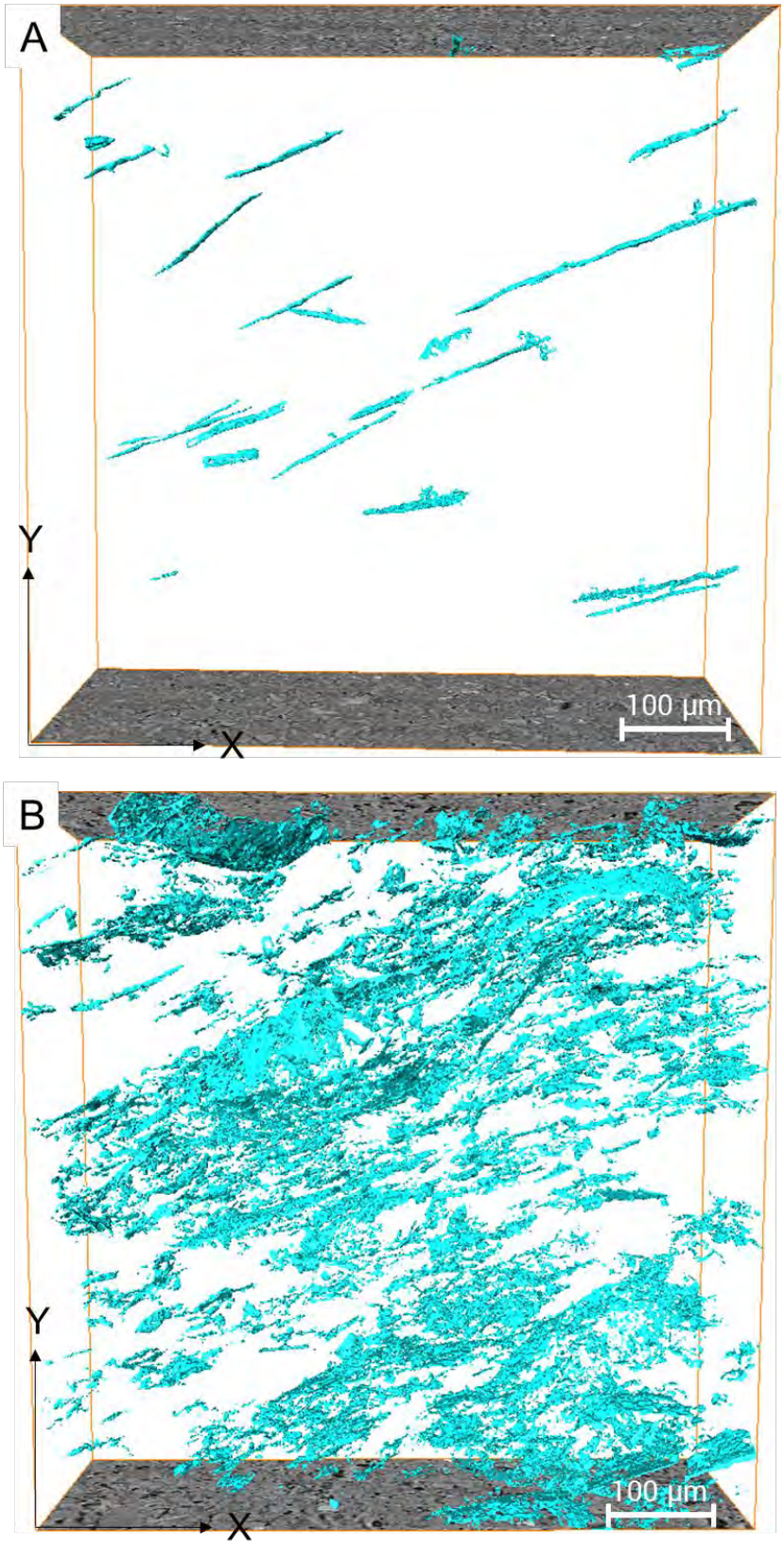

Figure 4.7: A 3D of subhorizontal microfractures in YX section, (A) sample A and (B) sample B

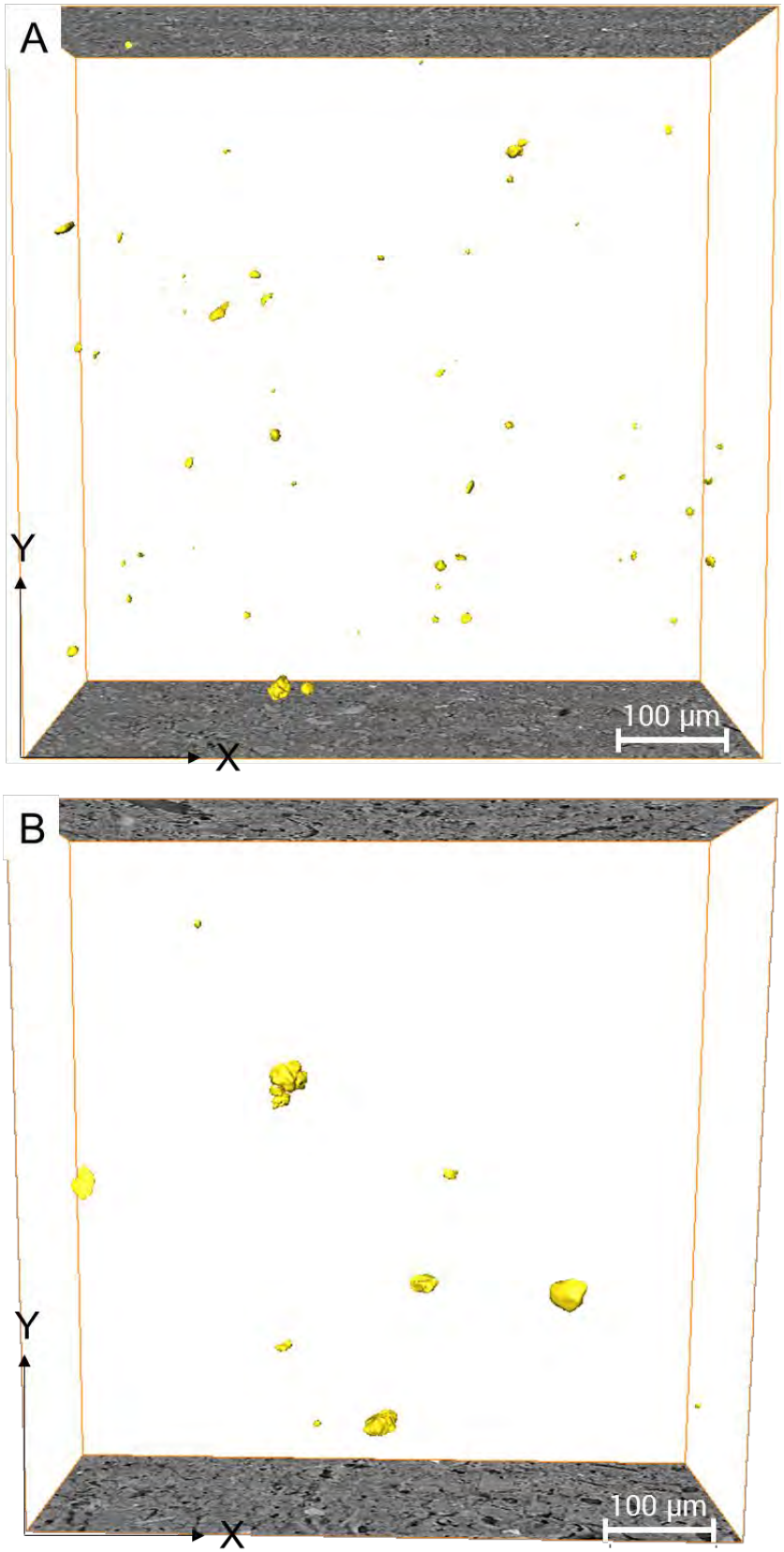

Figure 4.8: A 3D shape of pyrite distribute around show in YX section (A) sample A and (B) sample B.

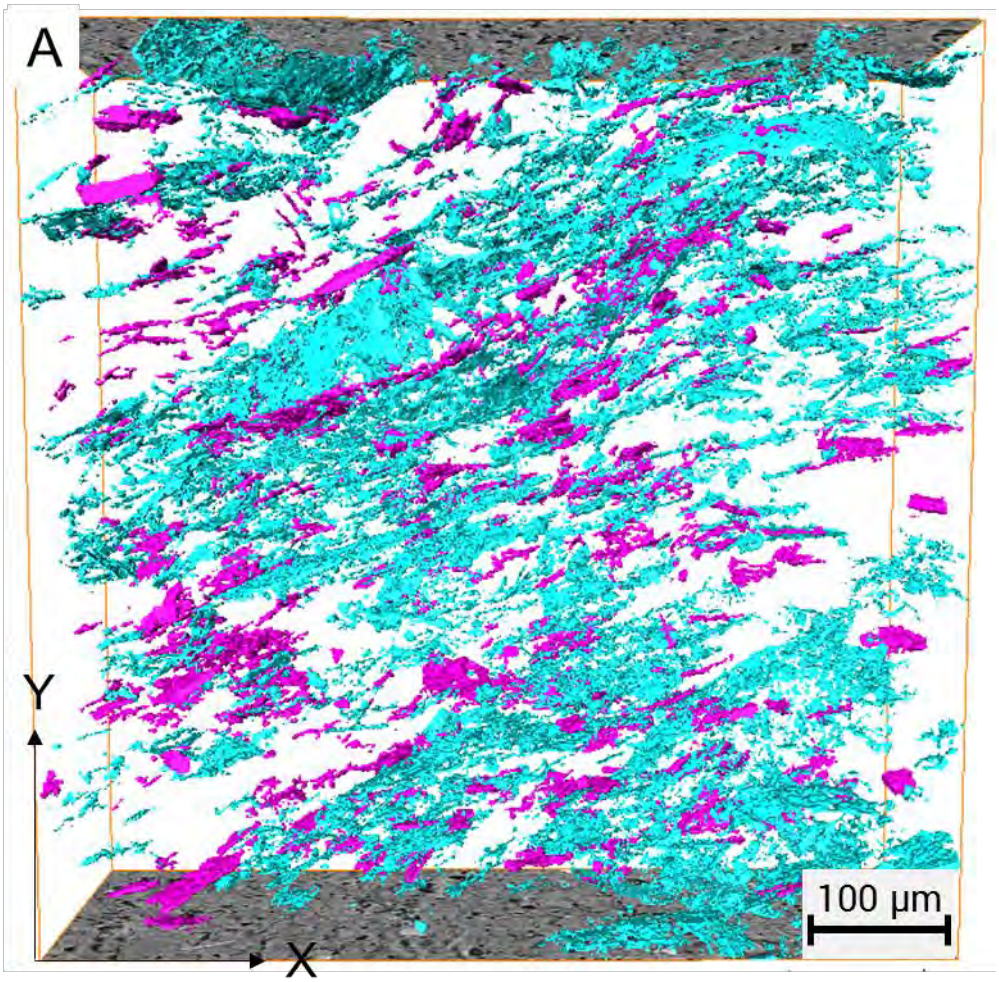

Figure 4.9: A 3D model shows microfractures (baby blue) and clay-particles (pink) are aligned parallel to each other in sample B

Chapter 5

Discussion

5.1 Mineralogy

As a previous study show lacustrine and fluvial deposits are interbedded in this area due to annual water supply (Water 1983). All sediments in Salton Sea are transported by Colorado river. Sands, silts, and clays are deposited in center of lake (Arnal 1961). The water contain calcium carbonate then calcium carbonate in the sediments is from precipitation or transportation by Colorado river (Arnal 1961). Consistent with Syn-XRD results, only sample A contain carbonate minerals such as calcite and dolomite, indicating that variation of fluids ejected from different periods of the same mud volcano. In addition, study by Brothers D. N. et al., (2009) show cross-section in Salton Sea (Figure 2.4) Pleistocene Brawley Formation which are mudstone, probably source of clay-rich fluids formed mud volcano in this area.

5.2 Clay fabrics and microstructures

For previous study about preferred orientation of clay minerals in shale, schist, fault gouge, and other clay-rich rocks (Wenk et al., 2010; Kanitpanyacharoen et al., 2010) suggested that clay minerals develop their preferred orientation during compaction, crystallization under stress, ductile deformation. The formation process of sedimentary rocks from mud volcano is quite different from those of other clay-rich rocks such as shale and mudstone, which are normally deposited in the subsurface. Due to slow cooling down on the surface. The results from both methods clearly show that preferred orientation of clay minerals in both samples are different. In sample A, clay minerals are very weak while moderate preferred orientation in sample B. Despite both samples were collected in the same area and contained similar clay contents but the alignment of clay-particles was different. Due to the grain size effect (Figure 5.1). Sand- or silt-size particles in the matrix play a major role in controlling the preferred orientation of sheet-like clay particles during sedimentation (Figure 5.2-5.3). The more sand- or silt-size particles, the more negative effect to the development of clay orientation.

For subhorizontal microstructures which are investigated by Syn-XTM (Figure 4.7), probably the results spaces between sheet-like clay particles during sedimentation process. Conformed by Figure 4.9 which sheet-like clay particles and microfractures are aligned parallel to each other. The sample A has less microfractures than those in sample B, because possibly filled by sand- or silt-size particles.

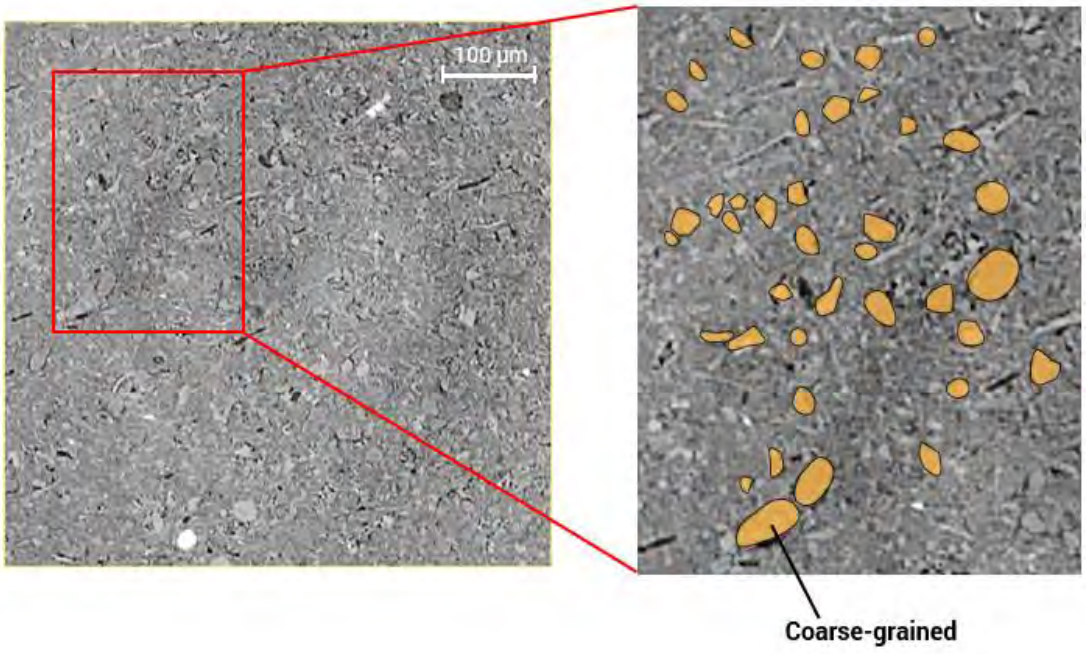

Figure 5.1: A microtomographic image of sample A shows that there are many coarse-grained of other minerals.

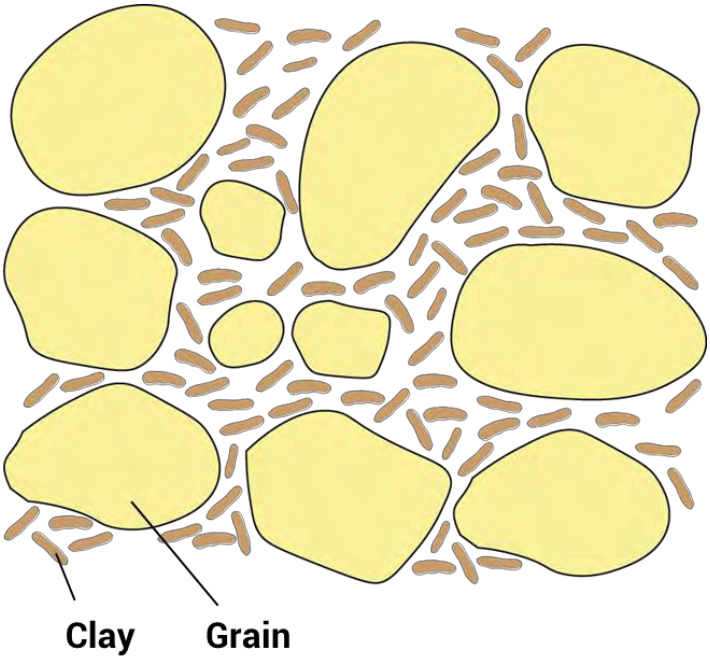

Figure 5.2: A sketching model show clay-particles are filled in spaces between grain like those appear in sample A.

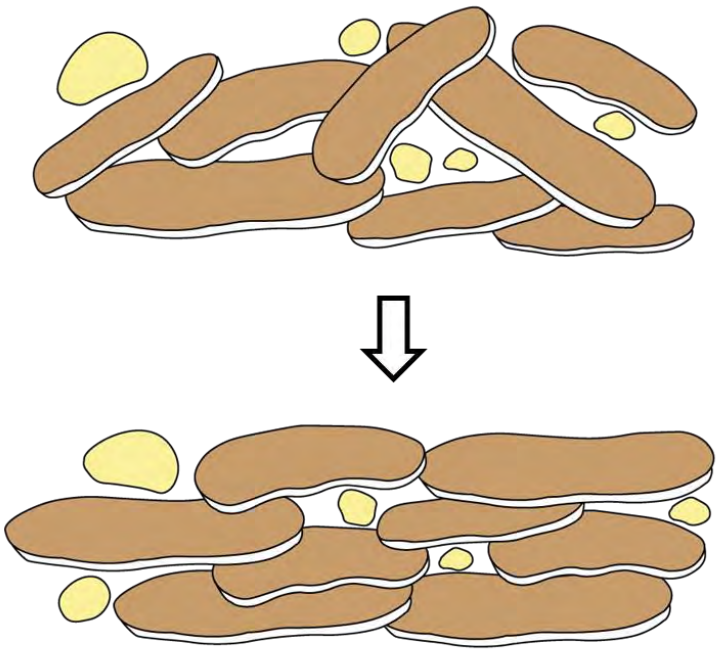

Figure 5.3: A sketching model show clay-particles aligned in the same direction like those appear in sample A.

5.3 Comparison with other clay-rich rocks in this area

- **SAFOD sample**

According to Salton Sea located directly on the San Andres Fault, the main tectonic process which forced the subsurface hot fluids exploded to surface is tectonic from San Andreas Fault. Then we compared the results with study by Janssen et al., (2012) about fault gauge from San Andreas Fault Observatory at Depth (SAFOD) samples. The samples are S1, S2, and S3. The compositions of samples are quite similar to Sample A and B such as clay and carbonate minerals (Table 6), indicating that origin of clay-rich sedimentary rock underground which clay-rich fluid in mud volcano melted from.

Clay fabrics from this study (Figures 5.4) show that only sample S2 has orientation of clay minerals with 1.1 – 1.3 m.r.d., which means most of clays are oriented randomly due to deformation during fault process.

Furthermore, supporting that the alignment of clay minerals in mud volcano samples does not affect from faulting process.

- **Davis-Schrimpf Mud Volcanoes**

Davis-Schimpf Mud Volcanoes are considered suface expressions of the Salton Sea Geothermal Systems as well as Salton Sea mud volcano. The location of Davis-Schrimpf Mud Volcanoes shows in Figure 5.5. Previous work by Sturz et al. (1992) analyzed clay compositions of Davis-Schtimpf mud volcanoes sample as 45-70% smectite, 20-35% illite, and 10-20% kaolinite. Rudolph and Manga (2010) also measured the component of 2 mud samples. Suggested that the minerals are kaolinite, muscovite, smectite, dolomite, calcite, and albite in both samples. And one of them composed with orthoclase. Constitute with the results from this study, indicating Davis-Schrimpf Mud Volcanoes and Salton Sea mud volcano are from the same origin.

Table 5.1: A compositional comparison with SAFOD samples

Minerals	Sample A	Sample B	S1	S2	S3
Illite-mica	56	36	-	-	-
Illite-smectite	-	12	22	38	47
Kaolinite	10	12	-	-	-
Smectite	7	9	-	-	-
Chlorite	2	-	-	12	-
Carbonate	10	-	5	4	-
Others	15	31	73	47	53

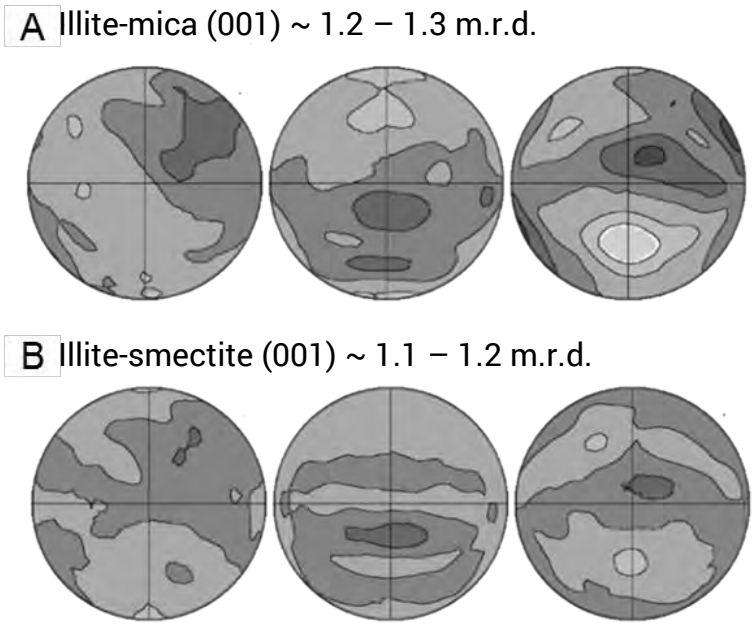

Figure 5.4: A pole figure of SAFOD sample S2 show that (a) illite-mica weak oriented in (001) and (b) illite-smectite weak oriented in (001) as well.

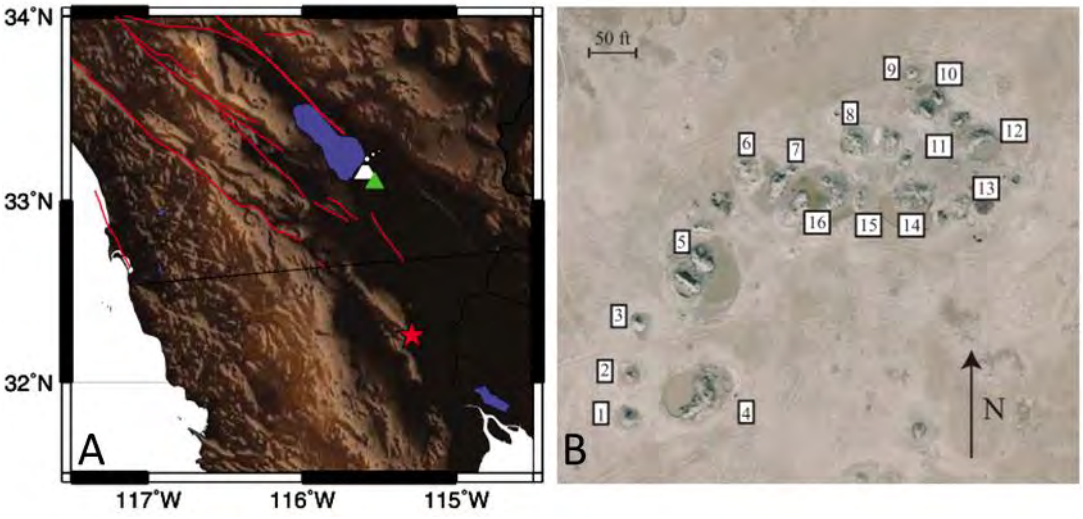

Figure 5.5: A location map of Davis-Schimpf Mud Volcanoes, (A) Red star indicates epicenter of E1 Mayot-Cucapah event. Green triangle is the location of Wildlife Liquefaction Array and white triangle is Davis-Schimpf Mud Volcanoes. (B) Aeral photograph of is Davis-Schimpf Mud Volcanoes.

Chapter 6
Conclusions

6.1 Conclusions

The goals of this study are to identify mineral compositions and orientation of mineral by using Synchrotron X-ray diffraction. According to the results, both sample consist of clay minerals about 69 – 75 wt.% with major phases e.g. illite-mica, smectite, and kaolinite and other minerals such as pyrite. For calcite and dolomite are found in only sample A. The orientation of minerals is calculated and shown as pole figure. Sample A has weaker degree of clay orientation that those in Sample B. In addition, the three-dimensional microstructures are investigated by using Synchrotron X-ray microtomography. The results show more clearly about the alignment of clay particles that affected by grain size. With zoom into micron scale show that coarse-grained in sample A are the negative effect to the development of clay minerals. Lastly, microfractures and clay-particles are aligned parallel to each other.

6.2 Future study

Due to seismic zone in Salton Sea, this area is sensitive about earthquake. This study about orientation of minerals can use for further study to more understand seismic anisotropy.

References

Arnal, R.E. Limnology, Sedimentation, and Microorganism of the Salton Sea, California, Geological Society of America Bulletin, Vol. 72, 427-478. 1961.

Brothers, D.S., Driscoll, N.W., Kent, G.M., Harding, A.J., Babcock, J.M., and Baskin, R.L. Tectonic evolution of the Salton Sea inferred from seismic reflection data, Nature geoscience, Vol. 2, 581-583. 2009.

Gilani, M.S., Boone, M.N., Mader, K., and Schwarze, F.W.M.R. Synchrotron X- ray micro-tomography imaging and analysis of wood degraded by *Physisporinus vitreus* and *Xylaria longipes*, Journal of Structural Biology 187, 149-157. 2014.

Helgeson, H.C. Geologic and thermodynamic characteristics of the Salton Sea Geothermal System, American Journal of Science, 266, 129–166. 1986.

Irwin W.P.Geology and plate-tectonic development. In R.E. Wallace (ed.), The San Andreas Fault System, California, 61-77. Washington : United States Government Printing Office, 1990.

Janssen, C., Kanitpanyacharoen, W., Wenk, H.-R., Wirth, R., Morales, L., Rybacki, E., Kienast, M.,and Dresen, G. Clay fabrics in SAFOD core samples, Journal of Structural Geology 43, 118-127. 2012.

Janssen, C., Wirth, R., Reinicke, A., Rybacki, E., Naunmann, R., Wenk, H.-R., and Dresen, G. Nanoscale porosity in SAFOD core samples (San Andreas Fault), Earth and Planetary Science Letters 301, 179-189. 2010.

Kanitpanyacharoen, W., Parkinson, D.Y., Carlo, F.D., Marone, F., Stampanoni, M., Mokso R., MacDowell, A., and Wenk, H.-R. A comparative study of X-ray tomographic microscopy on shales at different synchrotron facilities: ALS, APS and SLS, Journal of Synchrotron Radiation 20, 1-9. 2012.

Kanitpanyacharoen, W., Ketss, F.B., Wenk, H.-R., Wirth, R. Mineral preferred orientation and microstructure in the Posidonia Shale in relation to different degrees of thermal maturity, Clays and Clay minerals, Vol. 60, 315-329. 2012

Kerrick, D.M., M.A. McKibben, T.M. Seward, and K. Caldeira, Convective hydrothermal CO_2 emission from high heat flow regions, Chemical Geoleology 121, 285–293. 1995.

Lutterotti, L., Vasin, R. and Wenk, H.-R. Rietveld texture analysis from synchrotron diffraction images. I. Calibration and basic analysis, Powder diffraction, 29(1), 76-84. 2013.

Lachenbruch, A.H., Sass, J.H., and Galanis Jr., S.P. Heat flow in southernmost California and the origin of the Salton Trough, Journal of Geophysical Research, 90, 6709– 6736. 1985.

Mazzini, A. Mud volcanism: Processes and implications, Marine and Petroleum Geology 26, 1677-1680. 2009.

Muffler, L., and White, D. Active metamorphism of Upper Cenozoic sediments in the Salton Sea geothermal field and the Salton trough, southeastern California, Geological Society of America Bulletin, Vol. 80, 157-182. 1969.

Robinson, P.T., Elders, W.A., and Muffler, L.J.P. Quaternary volcanism in Salton Sea geothermal field, Imperial Valley, California, Geological Society of America Bulletin, 87, 347 – 360. 1976.

Rudolph, M.L., and Manga, M. Mud volcano response to the 4 April 2010 El Mayor-Cucapah earthquake, Journal of Geophysical Research, Vol. 115, 1-14. 2010.

Sturz, A., Kamps, R., and Earley, P. Temporal changes in mud volcanos, Salton Sea geothermal area, in Y. Kharaka and A. Maest (ed.), Water-Rock Interaction, 1363–1366, Balkema, Rotterdam : Netherlands. 1992.

Wenk, H.-R., Voltolini, M., Kern, H., Popp, T., and Mazurek, M. Anisotropy in shale from Mont Terri, The leading edge, 742-748. 2008.

Waters, M.R. Late holocene lacustrine chronology and archaeology of ancient Lake Cahuilla, California. Quaternary Research, Vol. 19, 373–387. 1983.

Williams, A.E. Fluid density distribution in a high temperature, stratified thermohaline system: Implications for saline hydrothermal circulation, Earth and Planetary Science Letters, 146, 121 – 136. 1997.